Research Square

Preprints are preliminary reports that have not undergone peer review.
They should not be considered conclusive, used to inform clinical practice,
or referenced by the media as validated information.

Physical Model Experimental Study on the Coalface Overburden Movement Law on the End-slope of an Open-pit Mine

xinpin ding (ccridxp@163.com)
China Coal Research Institute https://orcid.org/0000-0003-2614-5729
Fengming Li
China Coal Research Institute
Zhenwei Wang
North China University of Technology
Sheng Sang
China Coal Research Institute
Mingming Cao
China Coal Research Institute

Research Article

Keywords: end slope coal mining, strata movement, slope stability, physical model experiment, failure partition

Posted Date: January 13th, 2022

DOI: https://doi.org/10.21203/rs.3.rs-1208254/v1

License: This work is licensed under a Creative Commons Attribution 4.0 International License.
Read Full License

Abstract

Due to technology and safety limitations, the amount of coal resources overlying slopes in open pit coal mines is immense. In recent years, this problem has gradually attracted the attention of researchers. How to realize the efficient recovery of the side overburden resources with the premise of ensuring the stability and safety of the slope has become an important topic for the development of opencast mining technology in China. To study the yield failure characteristics of coal pillars and the rock mass migration law of the end slope mining field under the mining condition of the end slope shearer, 2D/3D, integrated, simulation experimental equipment is developed based on similarity theory and efficient region theory. This equipment overcomes the technical problem that the internal failure of the rock mass is invisible and that deformation data are not easily obtained during the simulation of end slope coal mining on an existing experimental platform. Based on the engineering geological conditions of the Ordos mining area in China, a typical engineering geological model of the slope near the horizontal condition is constructed to simulate the process “formation of mining cave group -failure of support coal pillars - instability of slope rock mass”. Based on laser positioning technology and multiangle, oblique photography technology, a panoramic phase 3D laser scanner, high-resolution digital camera and deep space micromonitoring system are comprehensively employed to carry out the whole process tracking monitoring and analysis of the deformation and failure of the supporting coal pillars and slope rock mass. The experiment is verified by numerical simulation. The results show that under the experimental conditions, with an increase in mining cave depth, the vertical stress of the supporting coal pillar increases linearly. At a certain distance before reaching the end of the mining cave, the peak value is reached. At this time, the depth continues to increase, and the stress value decreases sharply. The vertical stress gradually decreases to the original rock stress after a certain distance beyond the end of the mining cave. A certain length of supporting coal pillar from the end of the mining cave will never collapse, which is approximately 2.5~3 times the width of the mining cave. The triggering condition of slope deformation and failure is under the combined action of dynamic and static loads. The actual stress of the supporting coal pillar in the deep part of the geometric centre along the slope of the mining cave group is greater than the ultimate stress, and then large discontinuous deformation of multiple adjacent coal pillars around the central coal pillar is caused by compressive shear failure. The boundary of the final collapse plane range of the roadway group is approximately a closed curve formed by two paraboloids, which are axisymmetric with the No. □ coal pillar and open opposite. The parabola opening in the shallow part of the slope area is small, and the parabola opening in the deep part of the slope area is large. There is a significant space-time correspondence between the failure of supporting coal pillars and the deformation of the slope surface. According to the failure process of the rock mass structure and the movement and deformation characteristics of the slope surface, the slope after failure can be divided into three areas, and the upper part of the slope is the key area of deformation and instability of the overlying rock mass in the end-slope mining field. The research results provide a theoretical basis for scientific monitoring and stability control of slope deformation coal mining conditions in open-pit mines.

Introduction

By 2020, there were approximately 420 open-pit coal mines in China, accounting for 7% of the total number of coal mines in China, with a production capacity of 950 million tons, accounting for 18.6% of the total production capacity of coal mines in China. Restricted by mining technology, stripping ratio, slope safety and other factors, the amount of slope compaction resources in open-pit mining areas in China is vast[1,2]. The main reasons for these immense resources can be attributed to two aspects. First, most open-pit coal mines in China adopt the mining methods of zone mining, and trucks are transported along the loop line of the end slope and the inner dump overburden side slope. To ensure the stability of the slope, the overall range of the slope angle is only 20° ~ 35° under normal circumstances. After lateral exposure, the coal seam covered by the slope is buried again by the inner dump and causes a permanent loss. The resource loss phenomenon is more prominent in the open-pit mine group with seamless mining rights. Second, when open-pit mining is advanced to the deep area, the stripping ratio increases sharply, restricted by economic factors, and a large amount of coal covered by the end slope cannot continue to be mined by open-pit mining. According to this investigation, there are eight open-pit coal production bases and 40 open-pit mining areas in China, and more than half of the mining areas have more than 100 Mt of end slope pressing coal. In the Pingshuo mine area alone, the amount of resources covered by the boundary slope is approximately 0.1 billion t/km. Considering the Ordos coal field as an example, 157 open-pit coal mines are clustered; however, the area of a single open-pit mine is relatively small; its shape is irregular; and the amount of coal compressed by the blank area among mines, safety pillars, side coal and corner coal exceeds 500 million tons[3]. The large amount of resources covered by boundary slopes has caused invisible energy waste and economic loss to the national economy.

With dwindling coal resources and advances in mining technology, the problem of resources covered by boundary slopes in open-pit mines has gradually attracted attention in recent years, and how to efficiently recover these resources and minimize the waste of coal resources has become an important topic for the development of open-pit mining technology in China[4]. Of the many end-slope coal mining technologies, end shearer mining technology has been popularized and applied in countries such as the United States, Russia, and India as it lacks separate stripping or infrastructure, mining equipment is directly laid at the exposed position of the coal seam on the side of an open-pit mining site, and the whole mining process without support has a high recovery rate, low cost, good safety, strong adaptability and other characteristics[5-7]. Industrial tests have been performed in more than 10 mines in China[8,9]. Under the premise of minimal disturbance to the ecological geological environment, a large number of stagnant resources were recovered due to contributions to ecological protection and the high-quality development of coal mining areas in the middle and lower reaches of the Yellow River basin. Mining coal resources with this technology is carried out in the open pit, which has not realized the internal drainage; its essence is the process of mining roadway groups in the lower slope perpendicular to the slope trend, as the rock and soil weight of the upper slope are borne by the support coal pillar between the roadway during the whole mining process; if it is not controlled properly, it will very likely cause the failure of coal pillar and induce slope instability[10]. To ensure the safety of the slope under the premise of achieving the maximum coal mining, it is important to grasp the rock mass movement failure law and deformation instability mechanism of the end-slope mining field under the coupling effect of "open-pit mining" and

"roadway mining". The key is to use a reasonable size of supporting coal pillars of mining roadway groups. Many domestic and international scholars have carried out studies on the suitability assessment method of end slope coal mining[11-13], mining roadway group construction technology and equipment[14,15], recovery parameter design[16] and criterion for stability of coal pillar[17-19].
These research results provide a basis for scientific guidance of actual production; however, in the present stage, studies on the migration law of overlying rock masses of end-slope mining fields are focused on underground mining [20,21] or open-underground combined mining[22-24]. Relatively few studies address the failure process of coal pillars in the end-slope mining field and the deformation and movement law and instability mechanism of slope rock masses induced by coal pillar instability; the majority of the research methods are numerical analyses. Behrooz Ghabraie et al.[25,26] compared and analysed the application status of physical simulation and numerical analysis in mining engineering and concluded that physical simulation has obvious advantages in the study of strata movement, fracture propagation, collapse failure and gradual development of overburden deformation to the surface. The methods of similar material simulation experiment model construction, material selection and data acquisition were summarized systematically. Li ZK et al. [27,28] successfully realized the excavation of a complex cave under high-fidelity conditions by combining numerical analysis and physical simulation and obtained satisfactory test results. Zhu Jianming et al. [29-31] conducted theoretical analysis and simulation experimental study on rock mass deformation and failure mechanism under the coupling action of "key stratum" and conducted a comparative study on the difference of slope deformation and failure influenced by mining along slope dip and mining against slope dip in the recovery process of coal resources depressed by end slope in open-pit mine. Their study provides a basis for the optimization of temporal and spatial relations. The practice shows that the physical model experiment is an important method for studying the underground excavation induces movement and failure of overlying strata in the field of mining and geotechnical engineering, which can more accurately reproduce the whole deformation and failure process of a geologic body and can reflect the state of the occurrence and development of discontinuous deformation of rock mass. The method has the characteristics of simple process, visual, clear and direct effect, short cycle, quick effect, and repeated experiments. According to different research conditions, it has significant advantages in studying rock fracture failure, rock mass deformation and stress distribution evolution. In this paper, based on similarity theory, a 2d/3D integrated simulation experiment model of similar materials in end-slope mining field of open-pit mine is constructed based on the research background of coal mining in the Ordos area of China. The whole process of “formation of mining roadway groups - failure of supporting coal pillars - instability of slope rock mass” is simulated. By monitoring the full depth failure of the coal pillar and the surface movement and deformation of the slope, the formation process and evolution law of "enlarged pressure arch" in overlying rock mass of mining roadway groups were revealed. Based on the experimental results, the deformation and failure division of rock mass and the stage division of the moving failure process are carried out, and the key stage, trigger condition and key position of slope deformation and failure are proven, which provided a theoretical basis for slope stability control of an end-slope mining field in an open-pit mine.

General Situation Of Regional Engineering Geology

The Ordos coal field is the largest multiperiod coal field in China and one of the superlarge coal fields in the world. The coal field spans Shaanxi, Gansu, Ningxia, Inner Mongolia and Shanxi provinces and covers a width of 400 km from east to west and a length of 600 km from north to south. The plane of the coal field is slightly rectangular. The coal seam in the area has a stable occurrence, shallow burial, simple engineering geology and hydrogeology conditions and is suitable for open-pit mining. Therefore, there are many open-pit coal mines, resulting in a vast amount of overburden resources under the end slope. Consider an open-pit mine in Ordos for which end slope coal mining has been carried out. The engineering geological conditions and mining conditions of the mine are described as follows: (1) Two coal seams, No. 6 and No. 9, are overlaid by the end side slope; the thickness of the coal seam ranges from 14~17 m and 4~10 mm. The no. 9 coal seam is located in the lower part,; the distance between the two coal seams is 12~16 m; the false roof of the coal seam predominantly consists of clay rock, mudstone and sandy mudstone; the indirect roof is medium to fine grained sandstone; the bottom plate mainly comprises sandy mudstone; and the rock layers of the slope are hard to semihard rock. (2) The single step height of the end slope ranges from 12~15 m; the slope angle of the single step is in the range of 60° ~ 70°; the overall slope height ranges from 150~1180 m; the slope angle is in the range of 35° ~ 38°; the thickness of the quaternary loose stratum is ranges from 40~60 m; the slope mass and joint height is in the range of 150~180 m; and the slope stability is good. (3) First, an EML340-type side shearer is employed for mining the No. 9 coal seam, and the tunnel section is square. The height of the tunnel is equal to the thickness of the coal seam; the maximum depth is 240 m; and the width of the supporting coal pillar is 3.5 m. There is no support throughout mining. After the working face of the No. 9 coal seam is advanced a certain distance, the inner dump will follow up and backfill to the floor elevation of the No. 6 coal seam in time to prepare for the recovery of the coal seam. The typical engineering geological model of the end-slope mining field in the study area is shown in Figure 2.

Development Of An End Slope Coalmining Simulation Experimental Device And Experimental Design

2.1. Development of simulation experiment device

Similar material simulation experiments commonly utilized in geomechanics and mining engineering can be divided into two types: two-dimensional experiments and three-dimensional experiments. Two-dimensional experiments are often employed to reveal the deformation and stress distribution characteristics of typical geological sections. The work is small and economical, but the experimental results are often one-sided due to stress and boundary conditions. Three-dimensional experiments can obtain stress and deformation parameters in a full range with obvious defects such as invisible deformation and failure processes in rock masses. The deformation and instability of the end-slope mining field in open-pit mines is a typical problem of a three-dimensional space-time relationship.

Whether the simulation results can complement and verify each other by simultaneously carrying out two-dimensional and three-dimensional experiments and how to more scientifically reproduce the whole process of “formation of mining cave group -failure of support coal pillars - instability of slope rock mass”, aiming at the abovementioned problems, a simulation experimental device for end slope coal mining is developed on the basis of analysis.

2.1.1. Design of experimental platform

The experimental platform is a steel frame structure with a total weight of approximately 2.4 The platform is composed of a 2D simulation experiment area and a 3D simulation experiment area with dimensions of 1750 mm×250 mm×1200 mm and 1450 mm×1750 mm×1200 mm, respectively (Figure 3). The bottom of the platform is a steel plate with a thickness of 10 mm, and the lateral constraints are plexiglass plates with a thickness of 20 mm, which are bolted to the experimental bench. The higher strength provides effective lateral constraints for the model, and the stronger transparency is conducive to the collection and acquisition of experimental data. The glass panels on the front and rear sides of the 2D experimental area can be moved back and forth by adjusting the handwheel to realize the rapid addition and release of lateral constraints. The glass panel on the left side of the 2D experimental area and the glass panel in front of the 3D experimental area can be removed freely to create conditions for model excavation. Before the experiment, the constraints around the experimental platform were first installed and fixed, and the distance between the front and rear glass panels in the 2D simulation experiment area was adjusted to an appropriate position by adjusting the handwheel. The model was built layer by layer according to the similarity ratio. After the masonry work was completed, the glass panel on the left side of the 2D simulation experiment area and the glass panel on the front of the 3D simulation experiment area were removed. Simultaneously, the handwheel was adjusted to remove the constraints on the front and rear sides of the 2D simulation experiment area, and excavation and data collection were conducted after the simulated materials reached the predetermined strength.

2.1.2. Design of roadway groups construction device

To simulate the sequential excavation of roadway groups, a mining construction device is designed and developed on the basis of the experimental platform (Figure 4). The device includes two parts: a movable bracket and an impact shovel. The impact shovel is composed of a shovel handle and shovel head, which are made of steel. The cross-sections are square; the two sections are welded along the central axis; and the angle between the diagonal lines of the two sections is 45°. The shovel head is bevelled to form the shovel mouth; the four edges of the shovel mouth are polished to form the blade; and the side length of the shovel mouth can be flexibly configured as needed. The impact shovel is placed horizontally on the support with 3 groups of bearings. By adjusting the angle and distance between the two bearings in each set, the impact shovel can move back and forth along a degree of freedom (horizontal direction) without falling off under the action of external forces, and the height of the bracket can be adjusted by the height adjustment device. Using this device, a series of square roadway groups perpendicular to the slope trend can be constructed horizontally at the specified height of the model. The device has the

advantages of flexible position adjustment, the construction precision is controllable and the stress evolution characteristics of the surrounding rock are similar to the actual situation in the whole construction process.

2.2. experimental design and model construction

The self-developed 2D/3D integrated simulation experiment device is employed in this experiment. The mechanical property parameters and delamination thickness of the slope rock mass required by the experiment are shown in Table 1. Based on the engineering geological conditions of the study area and the size of the experimental platform, the similarity ratio parameters of the model are determined, as shown in Table 2. Clean fine sand is selected as the aggregate, and lime, gypsum and water are selected as cementing materials. Based on the physical and mechanical properties of the slope rock mass, the material ratio of each rock layer in the model is determined through a uniform experiment, as shown in Table 3. According to the distribution characteristics of the stratum and the ratio of similar materials, the model is laid horizontally layer by layer through mixing, paving and compaction. To achieve a better layering effect, the compaction thickness of a single layer is controlled between 1 and 2.75 cm, and mica powder is used to separate the layers. Considering the influence of the coal seam floor on the stability of the supporting coal pillar and the integrity of the system of "underlying strata - mining roadway groups - overlying strata" in the end-slope mining field, the model shall be laid at a depth of 100 mm below the coal floor, and it shall be as smooth as possible. The model sizes are 1750 mm×250 mm×930 mm and 1450 mm×1750 mm×930 mm.

Table 1 Main physical and mechanical property parameters of the rock and soil mass

Serial number	Lithology	Layer thickness （m）	Compressive strength （MPa）	Tensile strength （MPa）	Volumetric weight （t/m^3）
1	Loose layer	35	0.08	0.002	1.95
2	Fine-sandstone	8	50.7	2.8	2.35
3	Sandy mudstone	9.5	32.6	1.7	2.30
4	Coarse Sandstone	12	42.8	2.2	2.24
5	Sandy mudstone	18.5	32.6	1.7	2.30
6	Mudstone	6	18.5	1.4	2.44
7	Medium grained sandstone	18	45.5	2.5	2.27
8	Coarse Sandstone	6	42.8	2.2	2.24
9	Fine-sandstone	8	50.7	2.8	2.35
10	Sandy mudstone	6	32.6	1.7	2.30
11	Mudstone	5	18.5	1.4	2.44
12	No. 6 coal seam	15	10.6	0.8	1.40
13	Sandy mudstone	7	32.6	1.7	2.30
14	Mudstone	1.7	18.5	1.4	2.44
15	No. 9 coal seam	10	10.6	0.8	1.40
16	Sand-mudstone interbedded	20	45.5	2.6	2.42

Table 2 Similarity ratio of model to prototype

Similarity parameter	Geometry size	Volumetric weight	Strength
Ratio of similitude	1：200	1:1.6	1:320

Table 3 Material proportioning table of the model stratum

Layer No.	Lithology	Layer thickness (cm)	Ratio (Sand Lime Gypsum)	Ratio of aggregate to binder	Ratio of lime to gypsum
16	Loose layer	17.5	12:7:3	12:1	7:3
15	Fine-sandstone	4.0	8:5:5	8:1	1:1
14	Sandy mudstone	4.8	9:7:3	9:1	7:3
13	Coarse Sandstone	6.0	8:7:3	8:1	7:3
12	Sandy mudstone	9.3	9:7:3	9:1	7:3
11	Mudstone	3.0	10:8:2	10:1	8:2
10	Medium grained sandstone	9.0	8:7:3	8:1	7:3
9	Coarse Sandstone	3.0	8:7:3	8:1	7:3
8	Fine-sandstone	4.0	8:5:5	8:1	1:1
7	Sandy mudstone	3.0	9:7:3	9:1	7:3
6	Mudstone	2.5	10:8:2	10:1	8:2
5	No. 6 coal seam	7.5	9:8:2	9:1	8:2
4	Sandy mudstone	3.5	9:7:3	9:1	7:3
3	Mudstone	0.9	10:8:2	10:1	8:2
2	No. 9 coal seam	5.0	9:8:2	9:1	8:2
1	Sand-mudstone interbedded	10.0	8:5:5	8:1	1:1

2.3. Model excavation and data acquisition

2.3.1. Model excavation sequence and mining parameters

After the model material reaches the predetermined strength, the end slope is formed by open-pit mining, and the overall slope angle is 35°. Displacement monitoring targets are then laid on the surfaces of the 2D and 3D models. The 2D model displacement monitoring grid is laid at 150 mm×80 mm, and the 3D model targets are laid on the surface of each platform and slope body (**Figure** 5). Coal seam No. 9 recovery is then simulated. A total of 9 mining roadways are laid out in the 3D model, and homemade construction devices are utilized for mining roadway construction from right to left, with sizes of 50 mm×50 mm×1200 mm. The end of the roadway is located at the orthographic projection position of the top line of the slope at coal seam No. 9, and the width of the supporting coal pillar is 30 mm. To reduce the boundary effect, a 380 mm boundary coal pillar is installed on the left and right sides of the model.

The roadways are numbered from 1 to 9, and the numbers of supporting coal pillars are numbered from to .. The numbers of mining roadways and coal pillars are shown in Figure 6. According to the effective zone theory, after the 2D model is excavated to form a slope, first, the front and back sides of the coal seam are mined out, and only one central coal pillar is retained, with an initial width of 50 mm. The width of the coal pillar is gradually reduced by a gradient of 5 mm from both sides from outside to inside until the coal pillar reaches the bearing limit and compression failure occurs. The excavation design of the 2D model is shown in Figure 7. The marked units in **Figure** 5 to **Figure** 10 are mm.

2.3.2. Data collection methods and implementation steps

A panoramic phase, 3D laser scanner, high-resolution digital camera and deep space micro imaging system are employed to monitor the whole process of slope deformation and failure.

1) The panoramic phase, 3D laser scanner is used to carry out real scene scanning on the model surface at different stages to obtain mass point cloud data of the object surface with high precision. The measurement accuracy is 0.001 mm. Combined with the supporting point cloud processing software, the movement and deformation characteristics of the slope surface are obtained by comparing the two measured data before and after mining construction. In the whole process of the experiment, three panoramic scanning measurements are carried out on the surface of the 3D model slope. The scanning time is before mining roadway construction, after every 2 mining roadways are completed and the deformation is stable, and after all mining roadways are completed and the deformation is stable.

2) Based on multiangle tilt photogrammetry technology, high-resolution digital cameras are utilized to collect high-resolution images of two-dimensional models from different angles. A high-resolution orthophoto image of the model surface is then obtained through feature matching and extraction, encryption calculation and other steps. The movement and deformation characteristics of the overlying rock mass are obtained by comparing the points with the same name in different states. The frequency of high-resolution image acquisition is mainly determined by combining with the failure process of the upper rock mass of the supporting coal pillar.

3) A deep space micro imaging system is selected to track and monitor the failure and instability process of supporting coal pillars between two mining roadways, to obtain the initial position of collapse failure and its interlocking failure characteristics of supporting coal pillars about mining roadways, and to master the space-time corresponding relationship between the development process of coal pillars and the movement and deformation of slope surface. When each roadway reaches the predetermined depth, the micro camera is installed immediately. When each mining roadway reaches the predetermined depth, the micro camera is installed immediately. The equipment has the characteristics of its own light source, 160° wide angle, wireless transmission, etc., and continuous observation of surrounding rock deformation, and failure within 40 cm can be realized. With the continuous construction of the mining roadway, the installation and debugging of 9 pieces of equipment has been completed successively, numbered from A to I. The camera angles of A, C, E, G and I are towards the tunnel entrance, while the camera angles of B, D, F and H are towards the tunnel. During the experiment, the back and forth

movement along the axial direction of the roadway can be realized through the support rail. All image data can be displayed at the same terminal. Through online observation and graph comparison, the initial position and time of collapse failure of each supporting coal pillar can be obtained and recorded, and the failure range of the coal pillar group along the slope strike and inclination can be delineated accurately. The initial placement of the micro camera is shown in Figure 8.

Coal Pillar Yield Failure And Slope Rock Mass Movement And Deformation Law Of The End-slope Mining Field

3.1. Yield failure characteristics of supporting coal pillars in roadway groups

The yield failure tracking results of the supporting coal pillars in the 3D model experiment show that during the construction of the No. 1 to No. 3 mining roadways, no obvious compression deformation occurred in any coal pillar. In the construction process of the No. 4 roadway, the No. □ and No. □ coal pillars begin to be successively deformed at depths of 203 m and 198 m. With the subsequent construction of the roadway, the number of coal pillars with compression deformation gradually increases, and their magnitude expands significantly. When the construction of the No. 7 roadway is finished, the yield deformation of the No. □ coal pillar is significantly aggravated, and large pieces appear on both sides of the roadway (**Figure** 9 (c) and 9 (d)). At the end of roadway construction no. 8, coal pillar □ is the first to collapse at a depth of 196 m (**Figure** 9 (e) and **Figure** 9 (f)), and the No. □ and □ coal pillars on both sides of the roadway are immediately damaged by a chain reaction. In the construction process of the No. 9 roadway, the collapse range of the coal pillar group is further expanded around the location of the No. □ coal pillar, and the deformation of the overlying rock mass gradually develops to the surface. Along the slope direction, the coal pillar collapse spread to the no. □ and No. □ coal pillars. Along the slope tendency, the failure range of each coal pillar is enlarged, but the distance between the failure boundary of the deep region and the end of the roadway is similar, and the value is in the range of 25~30 m. Among all the coal pillars, the collapse range of the No. □ coal pillar in the middle is the largest, approximately 59.3 m. The boundary of the final collapse plane range of the roadway group is approximately a closed curve formed by two paraboloids, which are axisymmetric with the No. □ coal pillar and open opposite; the parabola opening in the shallow part of the slope area is small; and the parabola opening in the deep part of the slope area is large. During this experiment, the earliest collapse failure occurred in coal pillar No. □, which is located in the geometric centre along the slope strike. This coal pillar fails, which causes chain failure of other coal pillars on both sides. Therefore, the triggering condition of slope deformation and failure is under the combined action of dynamic and static loads. The actual stress of the supporting coal pillar in the deep part of the geometric centre along the slope of the mining roadway group is greater than the ultimate stress, and then large discontinuous deformation of multiple adjacent coal pillars around the central coal pillar is caused by compressive shear failure. The final collapse range of the supporting coal pillars is shown in **Figure 10.**

The deformation and failure characteristics of the supporting coal pillar and overlying rock in the 2D model experiment show that when the width of the coal pillar is gradually reduced to a 6 m by 1 m

gradient from the front and back sides of the model, the coal pillar collapses suddenly in the middle and deep regions as it has reached the ultimate strength under load, and the length of the failure range rapidly expands to 65 m along the slope tendency. However, no damage occurred from the deep area to the end of the mining roadway, which comprises a length of approximately 23 m. The overlying rock mass sinks immediately after pillar collapse, and the cracks and deformation rapidly spread to the surface. It can be seen from the comparative analysis that the yield failure characteristics of the supported coal pillar observed in the 2D and 3D model experiments are similar, that coal pillar collapse occurs in the middle and deep parts of the slope tendency, and that there is no damage at the end of a certain length range (Figure 11). The results of the numerical analysis show that the vertical stress of the supporting coal pillar shows obvious regularity with different depths. From the outside of the roadway, the maximum vertical stress of the coal pillar increases linearly with an increase in tunnel depth, and the peak value reaches approximately 4.7 MPa at a depth of roadway of 195 m. As the depth continues to increase, the stress value decreases sharply. When it goes beyond the end of the roadway to a certain distance, it gradually decreases to the original rock stress. The coal pillar failure area is located at depths in the range of 150~215 m of mining roadway. The numerical analysis shows that the length of the undamaged area at the end of the coal pillar is approximately 25 m, 2.5 times the width of the mining roadway, which is consistent with the model experimental results[32]. A curve showing the changes in the vertical stress of the coal pillar with the depth of the roadway is shown in Figure 12.

3.2. Temporal and spatial correspondence between coal pillar failure and slope surface deformation

The deformation of the slope surface is caused by the failure of the coal pillar in the end-slope mining field, and there is an obvious space-time correspondence between them. In time, after the chain failure of the supporting coal pillar, the upper rock mass collapses, and the deformation gradually develops to the surface. A vertical deformation concentration area with the shape of approximately an "ellipse" is formed in the geometric centre along the strike of the slope, and the long axis extends along the slope. The hinged structure formed as the rock sinks creates a horizontal thrust on the lower slope rock mass, resulting in horizontal deformation towards the open surface, while the upper slope body deforms along the slope due to the loss of lateral support, and the deformation process is relatively slow. The surface deformation cloud atlas of the slope surface and the typical monitoring point deformation curve obtained by physical simulation are shown in Figures 13 and 14, respectively. As shown in the graph, in the middle region, the slope surface is dominated by vertical deformation with a magnitude of approximately 0.38 m, while in the lower region, the slope surface is dominated by horizontal deformation with a magnitude of approximately 0.20 m. However, the horizontal deformation and vertical deformation on the upper slope surface are both significant with magnitudes of approximately 0.36 m and 0.32 m, respectively.

The spatial correspondence between the failure zones of coal pillars and the surface deformation zones of the slope is shown in Figure 15. In space, compared with the collapse area of the supporting coal pillar, the vertical subsidence basin in the middle of the slope deviates towards the free face. Under this experimental condition, the centre of the subsidence basin is located at the surface of the shallow boundary of the coal pillar failure area. The main reason is that due to the coupling effect of the stress

field of the "slope" and "mining roadway group", the stress is released in advance in the relatively thin area of the overlying rock mass during the process of rock mass deformation and failure extending to the surface. The deformation and failure characteristics of the slope rock mass obtained by numerical analysis are shown in Figure 14. The black arrow in the figure is the rock mass deformation vector. We intuitively determine the movement and deformation of the rock and soil mass of the slope. The influence range of end slope coal mining on the slope reaches approximately 100 m beyond the top line of the slope. The subsidence deformation of the rock mass shows obvious deviation towards the free face of the slope during the process of upwards expansion. The results of physical simulation and numerical analysis show agreement with the field monitoring data. The spatiotemporal correspondence between the failure of coal pillars and the surface deformation of the slope provides a theoretical basis for the monitoring and stability control of slope deformation.

3.3. Deformation and failure zones of the overlying rock mass and slope surface

The yield failure characteristics of the coal pillar in the end-slope mining field determine the movement and deformation characteristics of the overlying rock mass and the surface of the slope. The comprehensive analysis shows that under the condition of near-horizontal strata, the deformation and failure of the slope rock mass show obvious zoning characteristics under the influence of roadway construction. The overlying rock mass of the slope can be divided into three zones, A, B and C, by the fracture boundary of the moving basin and the boundary of the separation range (Figure 17).

(1) Zone A: located outside the fracture boundary of the moving basin at the bottom of the slope, the rock mass in this area is subjected to the horizontal thrust caused by key block rotary instability and sliding instability of zone B. It is easy to move horizontally towards the open surface of the slope, and the rock mass of the slope mainly undergoes horizontal deformation.

(2) Zone B: located directly above the failure zone of the supporting coal pillar, between the fracture boundary of the moving basin on the lateral side of the slope and the boundary of the separation range inside the slope. This area is formed gradually due to the collapse of the supporting coal pillar and the expansion of rock mass settlement to the surface, and the rock mass of the slope mainly undergoes vertical deformation.

(3) Zone C: located between the fracture boundary of the moving basin and the boundary of the separation range inside the slope. Due to the loss of the lateral support of the rock mass in zone B, deformation occurs along the slope. Therefore, both the horizontal movement and vertical movement characteristics of the rock and soil mass are obvious. This area is the key area for slope deformation and instability in the end-slope mining field. When the slope body is composed of rock steps and the rock surface is nearly horizontal or inclined to the slope surface, the rock and soil mass may slip along the interface of the weak rock stratum. When the upper part of the slope consists of a loose layer or other loose materials, circular sliding instability in the loose materials may occur in the rock and soil mass.

Conclusion

(1) A 2D and 3D integrated simulation experiment device is developed for end slope coal mining; a typical engineering geological model of end-slope mining field is established; the whole process simulation of "formation of mining roadway group - failure of supporting coal pillar - instability of slope rock mass" is realized; the yield failure characteristics of supporting coal pillars and the movement and deformation law of slope rock mass in an end-slope mining field under near-horizontal conditions are proven.

(2) The triggering condition of slope deformation and failure is under the combined action of dynamic and static loads. The actual stress of the supporting coal pillar in the deep part of the geometric centre along the slope of the mining roadway group is greater than the ultimate stress, and then large discontinuous deformation of multiple adjacent coal pillars around the central coal pillar is caused by compressive shear failure. The boundary of the final collapse plane range of the roadway group is approximately a closed curve formed by two paraboloids, which are axisymmetric with the central coal pillar and open opposite. The parabola opening in the shallow part of the slope area is small, and the parabola opening in the deep part of the slope area is large. However, the supporting coal pillar will not collapse in a certain length range at the end of the roadway, which is approximately 2.5~3 times the roadway width.

(3) Under the condition of near-horizontal rock strata, there is an obvious spatiotemporal correspondence between the failure of the coal pillar and the deformation of the slope surface, and the failure of the slope rock mass shows obvious zoning characteristics. The slope under the end slope coal mining condition can be divided into three zones according to the moving characteristics of the rock mass: the upper part of the slope is the key area of deformation and instability, and the potential failure mode of the slope is bedding slide or circular slide. The results of the physical simulation and numerical analysis show agreement with the field monitoring data, which provides a theoretical basis for the deformation monitoring and stability control of slopes under end slope coal mining conditions.

Declarations

Acknowledgements

This study was financially supported by the National Natural Science Foundation of China(Grant 51774184).

Conflict of interest statement

We declare that we have no financial and personal relationships with other people or organizations that can inappropriately influence our work submitted.

References

[1]BAI Runcai, Liu Chuang, Xue Yingdong, et al. Coordination mining technology for coal underlying the slopes between two adjacent open pits [J].Journal of China Coal Sooiety,2014,39 (10) :2001-2006.

[2]ZHANG Zhi,LIUChuang, Xue Yingdong, et al. Coordination mining technology of coal under side slopes in crossed limit area of two adjacent open pits [J].Coal Science and Technology, 2013, 41(9): 91-95.

[3]CAO Chunjie.Discussion on mining technology of surface mine group in Erdos area [J].Coal Engineering,2012(12):16-18.

[4]LI Chong,CAI Qingxiang,YUAN Yingjue,etal. Assessment of feasibility of leftover coal mining in end-slope of surface mine[J].Journal of Mining & Safety Engineering,2011,28(02):263-266+272.

[5] Sungsoon mo, Chengguo Zhang, Ismet Canbulat, et al. A Review of Highwall Mining Experience andPractice[C].Proceedings of the 16th Coal Operators' Conference, Mining Engineering, University of Wollongong, 2016: 522-530.

[6] Porathur JL, Karekal S, Palroy P. Web Pillar Design Approach for Highwall Mining Extraction[J]. International Journal of Rock Mechanics and Mining Sciences, 2013, 64(12): 73-83.

[7] Porathur JL,Srikrishnan S,Verma CP, et al. Slope Stability Assessment Approach for Multiple Seams Highwall Mining Extractions[J]. International Journal of Rock Mechanics and Mining Sciences, 2014, 70(7): 444-449.

[8]LIU Wengang, WANG Leishi, FU Qiang SHM highwall mining technology and key issues of application[J].Coal Engineering,2012(06):1-4.

[9]ZHANG Shuai,ZHANG Quntao,YUE Ting,etal.Application analysis of highwall miner for surface mine mining in China[J].Coal Technology,2016,35(06):233-235.

[10]LIU Yong,CHE Zhaoxue,LI Zhiqiang,etal. Analyses of end slope remnant coal mining and slope exposure time[J].Journal of China University of Mining & Technology,2006(06):727-731.

[11]Seib W.-T.. Advances in highwall mining[C]//3rd Large Open Pit Mining Conference, Mackay, Queensland, 1992: 145-150.

[12]Shen b Duncan-Fama-ME. Review of highwall mining experience in Australia and a case study[J]. Aust Geomech , 2001, 36(2): 25-32.

[13]Elmouttie M,Karekal S. A Framework for Geotechnical Hazard Analysis in Highwall Mining Entries[J]. Procedia Engineering, 2017, 191: 1203-1210.

[14] Ross C,Conover D,Baine J. Highwall Mining of Thick, Steeply Dipping Coal – a Case Study in Geotechnical Design and Recovery Optimization[J]. International Journal of Mining Science and Technology, 2019, 29(5): 777-780.

[15]Luo X,Ross J,Hatherly P, et al. Microseismic Monitoring of Highwall Mining Stability at Moura Mine, Australia[J]. Null, 2001, 2001(1): 1-6.

[16] Porathur JL, Karekal S, Palroy P. Web Pillar Design Approach for Highwall Mining Extraction[J]. International Journal of Rock Mechanics and Mining Sciences, 2013, 64(12): 73-83.

[17]CHEN Yanlong, WU Haoshuai.Catastrophe instability mechanism of rib pillar in open-pit highwall mining[J]. Journal of China University of Mining & Technology,2016,45(05):859-865.

[18]Porathur JL,Srikrishnan S,Verma CP, et al. Slope Stability Assessment Approach for Multiple Seams Highwall Mining Extractions[J]. International Journal of Rock Mechanics and Mining Sciences, 2014, 70(7): 444-449.

[19]Adhikary D,Shen B,Fama M. A Study of Highwall Mining Panel Stability[J]. International Journal of Rock Mechanics and Mining Sciences, 2002, 39(5): 643-659.

[20] QIAN Minggao ,XU Jialin.Behaviors of strata movement in coal mining[J]. Journal of China Coal Society ,2019,44(4):973-984.doi ;10.13225/j.cnki.jccs.2019.0337

[21]QIAN Minggao, XU Jialin. Behaviors of strata movement in coal mining[J].Journal of China Coal Society,2019,44(4) :973-984.

[22]SUN Shiguo ,WANG Sijing.Study of sliding mechanism for slope due to the excavation from open pit into underground mining[J].Chinese Journal of Rock Mechanics and Engineering,2000,19(1):126-129.

[23]DING Xinpin, WANG Zhenwei, LI Wei. Dynamic process and typical deformation-failure mechanism of mining slope[J]. Journal of China Coal Society,2016,41(10):2606-2611.

[24]DING Xinpin,LI Fengming,LI Hongyan,etal. Study on formation mechanism and evolution model about sliding surface of the bedding rock mining slope[J]. Journal of Mining & Safety Engineering,2020,37(05):1019-1026.

[25]Behrooz Ghabraie, GangRen, JohnSmith,etal.Application of 3D laser scanner, optical transducers and digital image processing techniques in physical modelling of mining-related strata movement[J]. International Journal of Rock Mechanics & Mining Sciences, 2015,80: 219-230.

[26]Sun T,YueZ,GaoB, etal. Model test study on the dynamic response of the portal section of two parallel tunnels in a seismically active area[J]. Tunn Undergr SpaceTechnol. 2011;26(2)391-397.

[27]Li ZK,Liu H,Dai R,etal.Application of numerical analysis principles and key technology for high fidelity simulation to 3-D physical model tests for underground caverns. Tunnelling and Underground Space Technology, 2005:20(4)390-399.

[28]WeishenZ,YongL,ShucaiL,etal.Quasi-three-dimensional physical model tests on a cavern complex under high in-situ stresses[J].Int J Rock Mech Min Sci. 2011;48(2)199-209.

[29]ZHU Jianming,LIU Xianquan,WU Jianping,et al. Similarity simulation on slope stability under condition of combined open and underground mining[J].Journal of Engineering Geology,2009,17(2):207-211.

[30]DING Xinpin, LI Shaochen, WANG Jun,etal. Optimization of underground mining development direction about end slope coal pillar recovery of open-pit coal mine[J].Journal of China Coal Society,2013,38(11):1923-1928.

[31]DING Xinpin,WANG Jun,LI Wei,et al. Analysis of slope sliding depth for open-underground combined mining under coupling effects about key strata[J]. Journal of China Coal Society,2014,39(S2):353-358.

[32] DING Xinpin ,LI Fengming ,FU'Tianguang,et al.Overburden movement and failure law of coalface in end slope and the slope stability control method[J].Journal of China Coal Society ,2021 ,46(9):2883-2894.

Figures

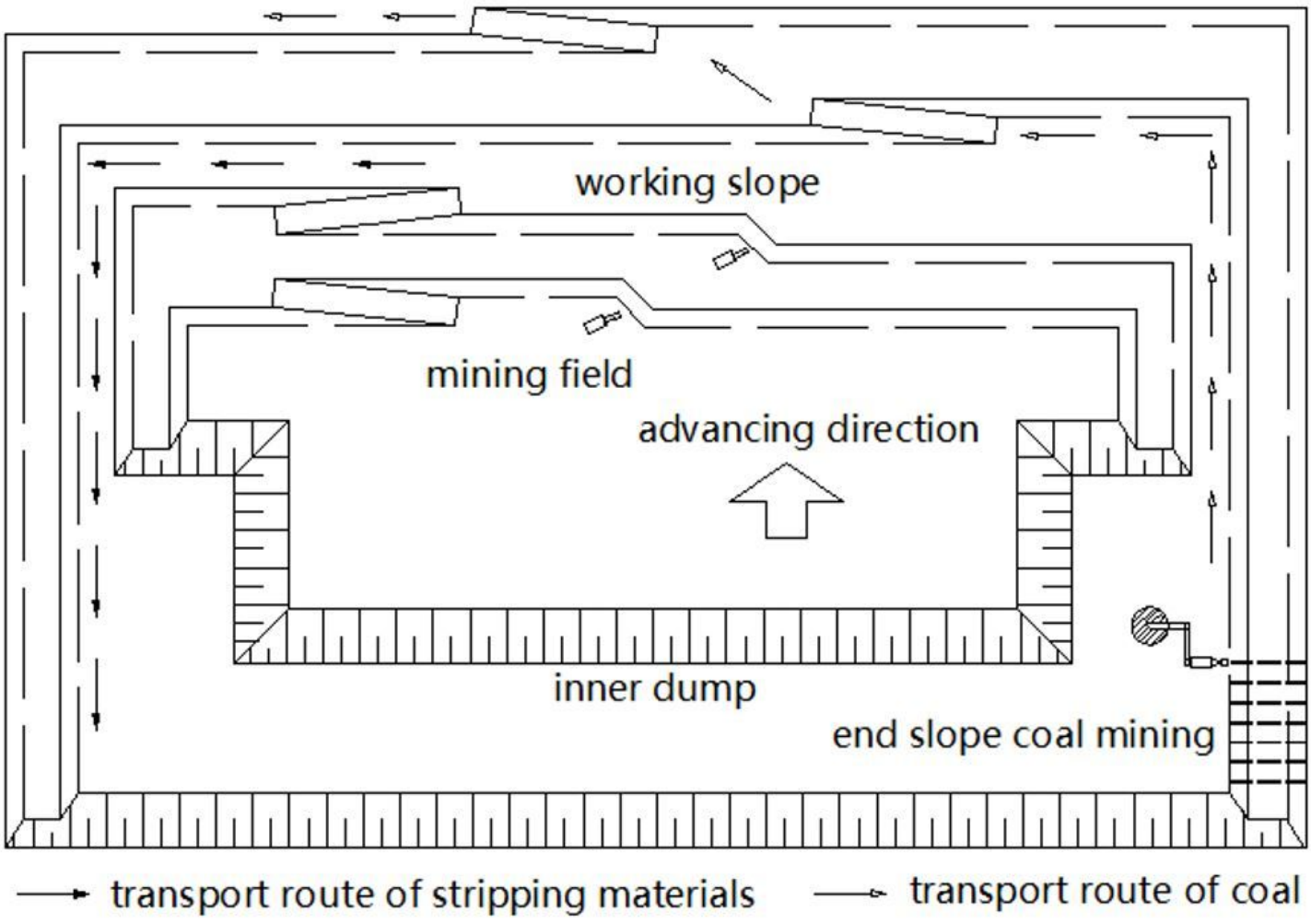

Figure 1

Diagram of the working face layout of end slope coal extraction in an open-pit mine

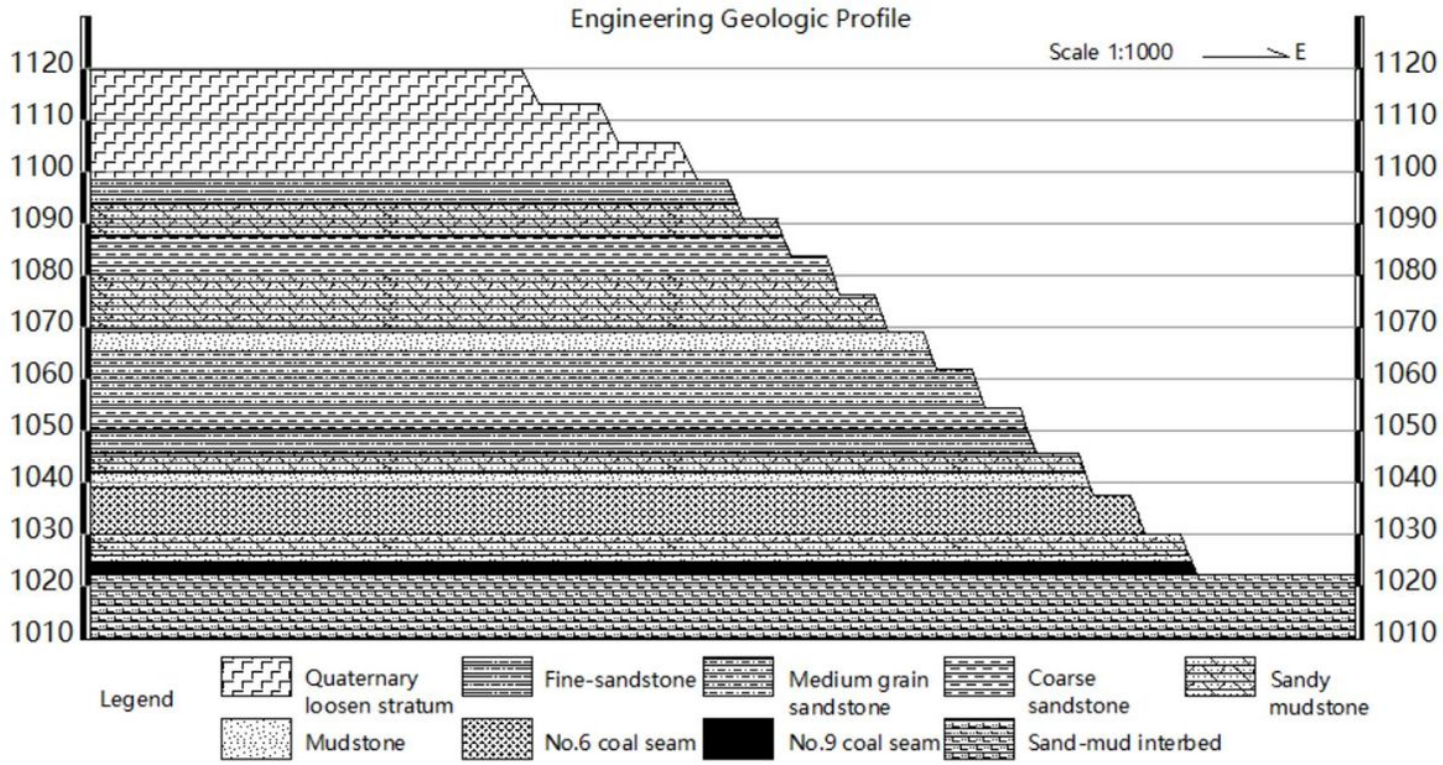

Figure 2

Typical engineering geological model of the end slope

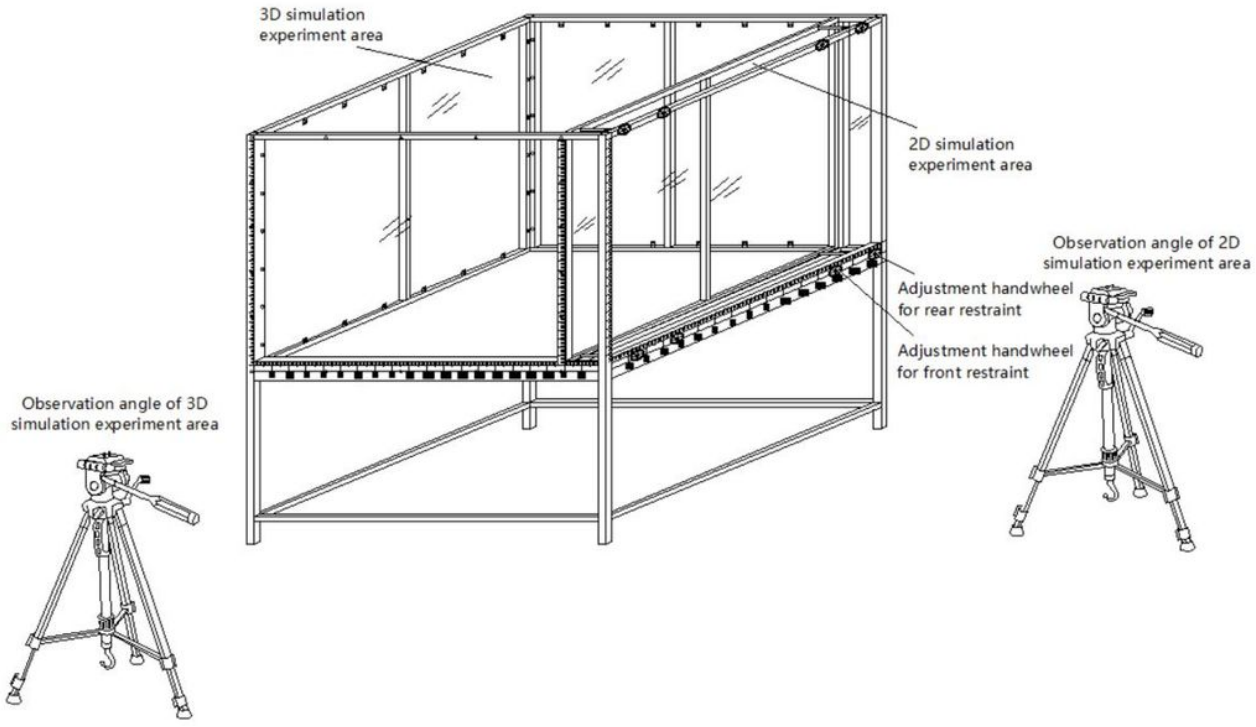

Figure 3

Diagram of the 2D/3D integrated simulation experimental platform of coal extraction in the end slope

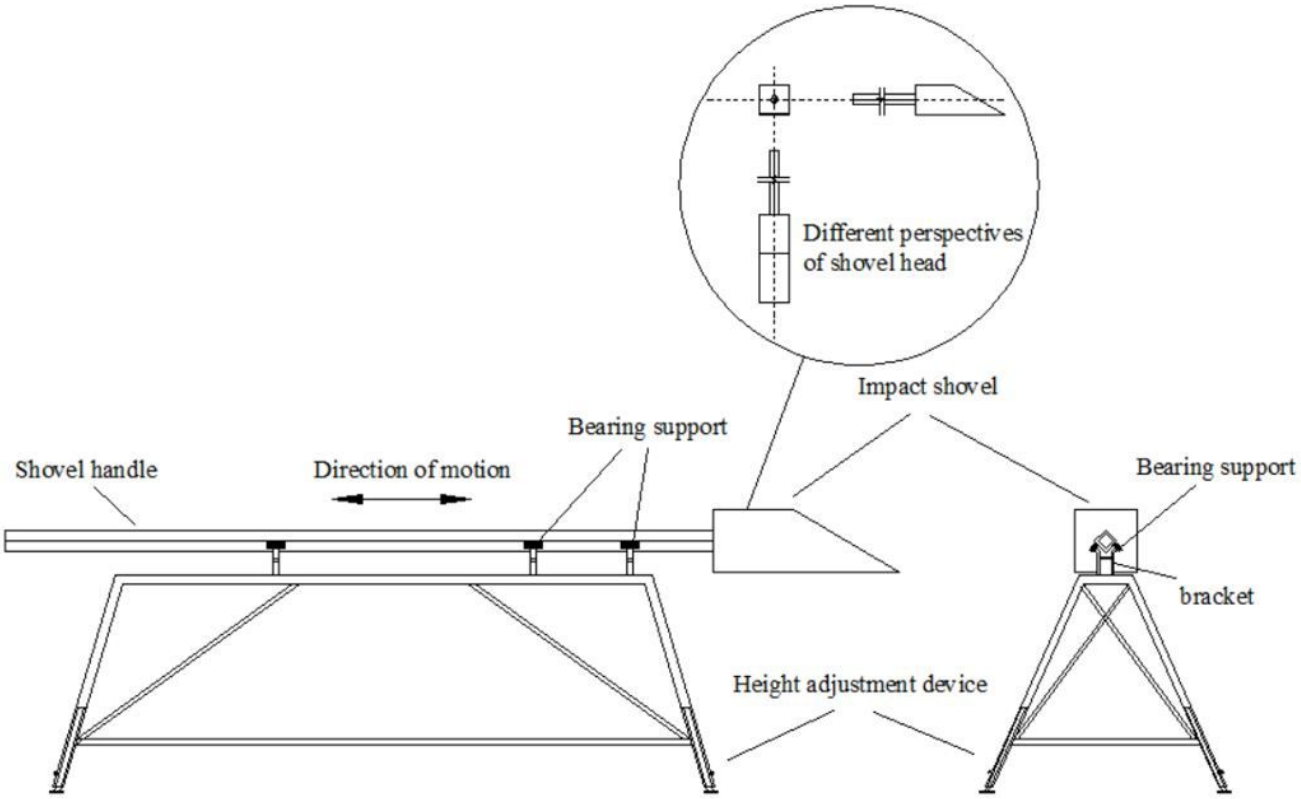

Figure 4

Diagram of roadway construction device

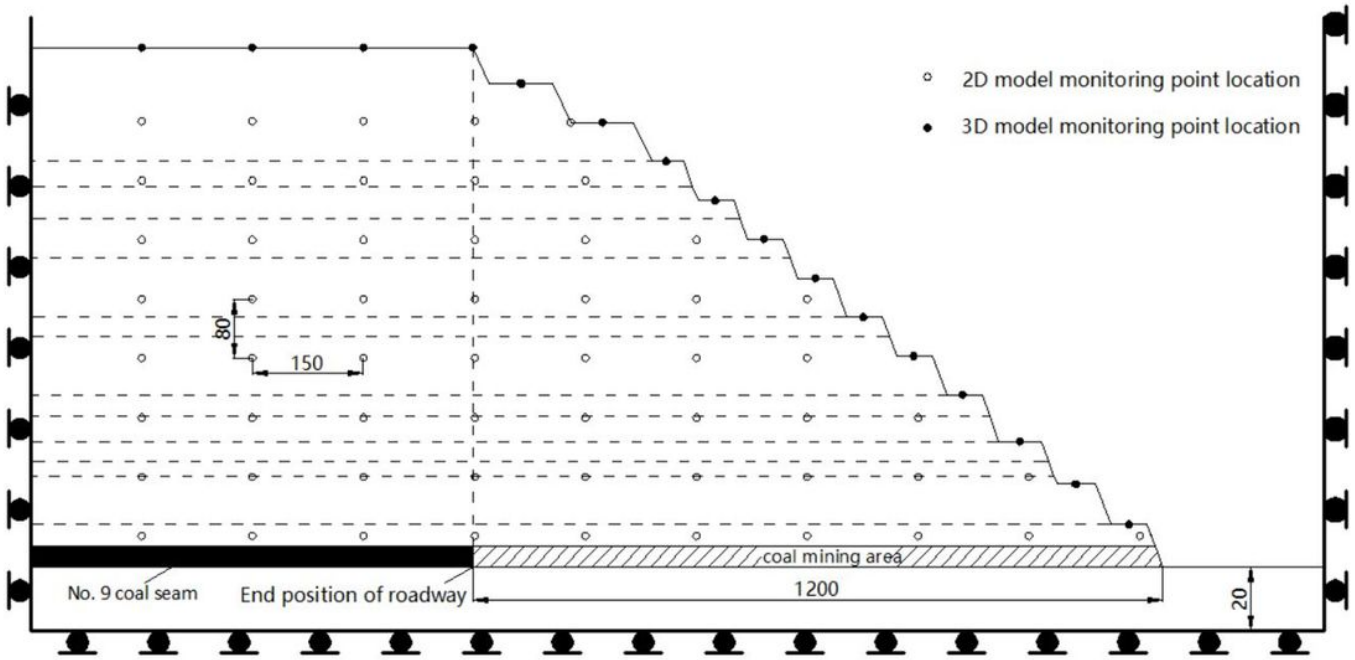

Figure 5

Diagram of monitoring point layout in the model section

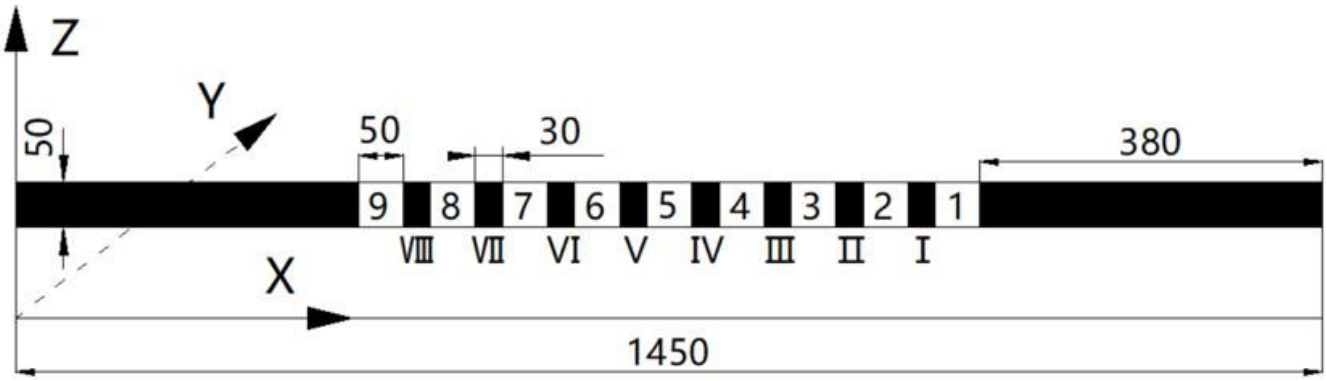

Figure 6

Numbered diagram of roadway and coal pillar

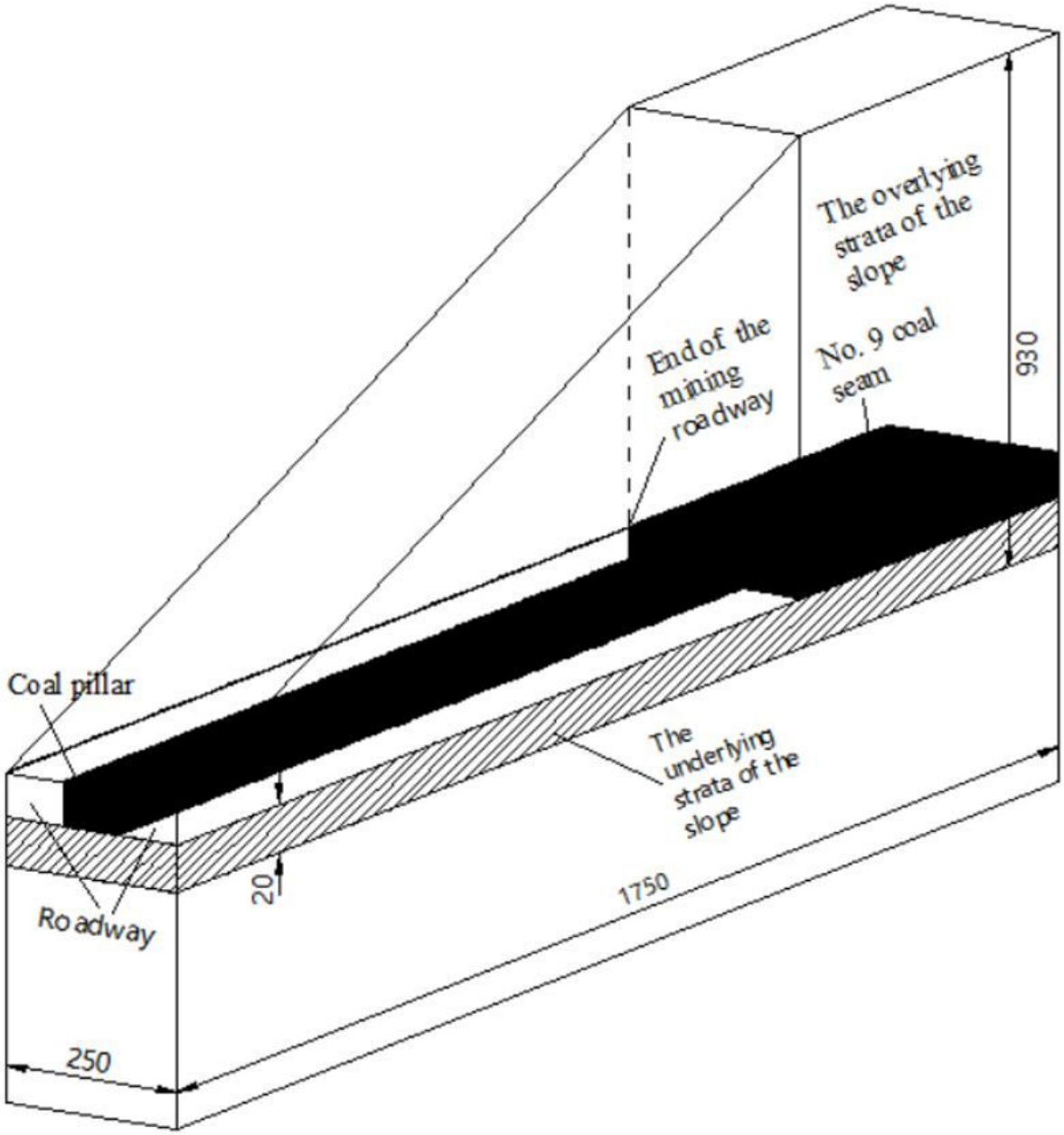

Figure 7

Excavation diagram of 2D model

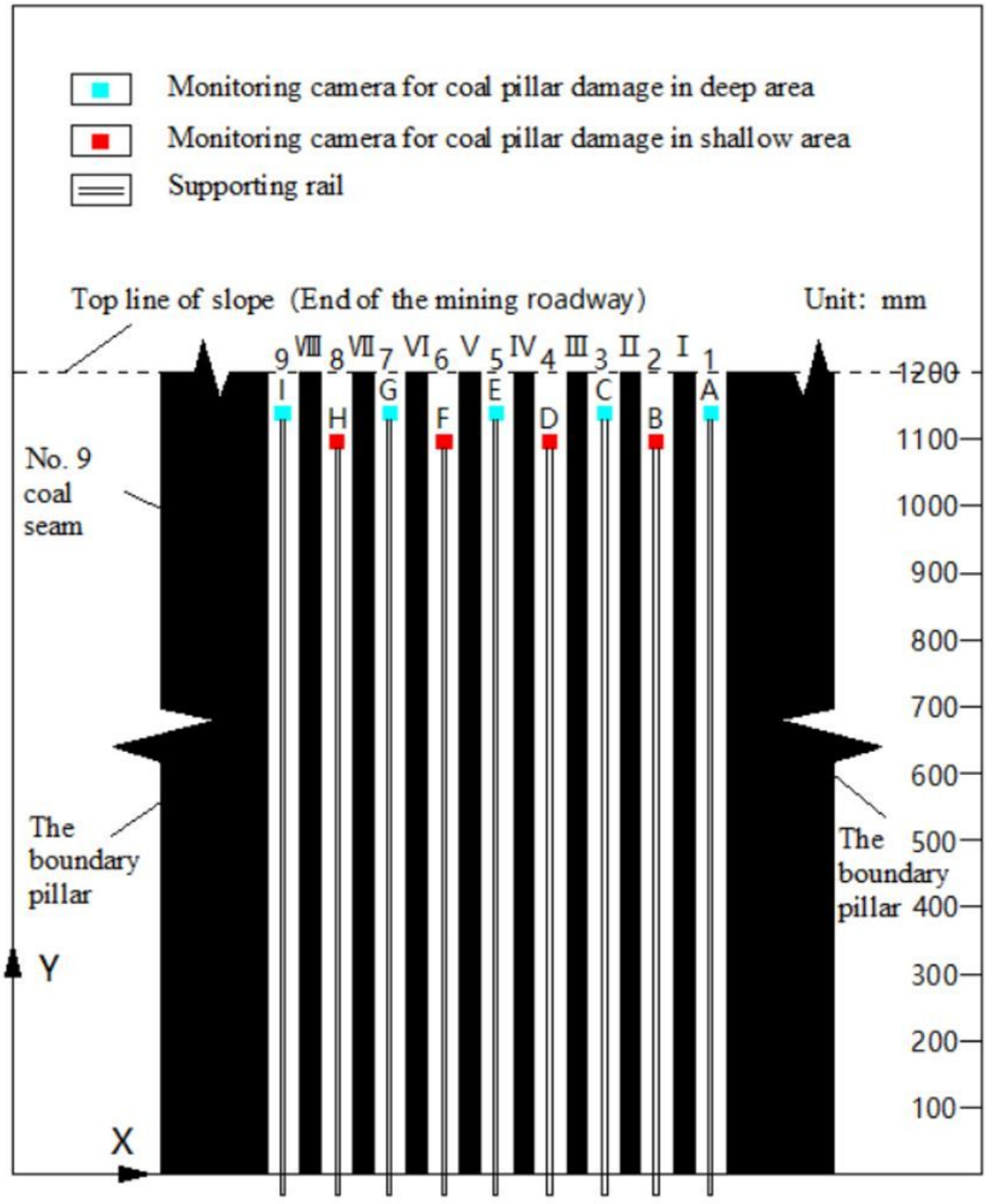

Figure 8

Diagram of the initial placement of the miniature camera

(a) Image of camera A after the end of mining roadway construction No. 3
(b) Image of camera C after the end of mining roadway construction No. 3

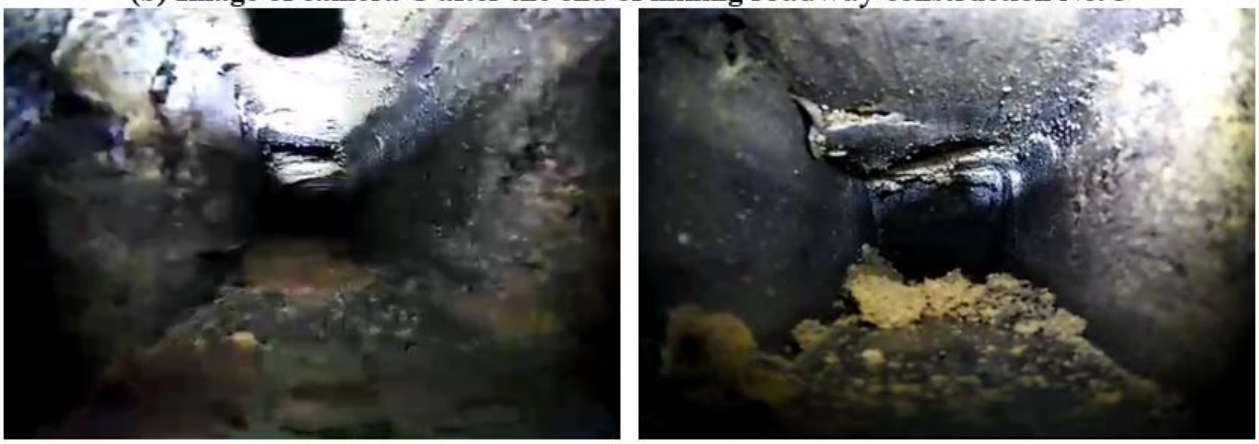

(c) Image of camera D after the end of mining roadway construction No. 7
(d) Image of camera E after the end of mining roadway construction No. 7

(e) Image of camera D after the end of mining roadway construction No. 8
(f) Image of camera E after the end of mining roadway construction No. 8

Figure 9

Yield failure characteristics in the typical position of the coal pillar about the roadway group

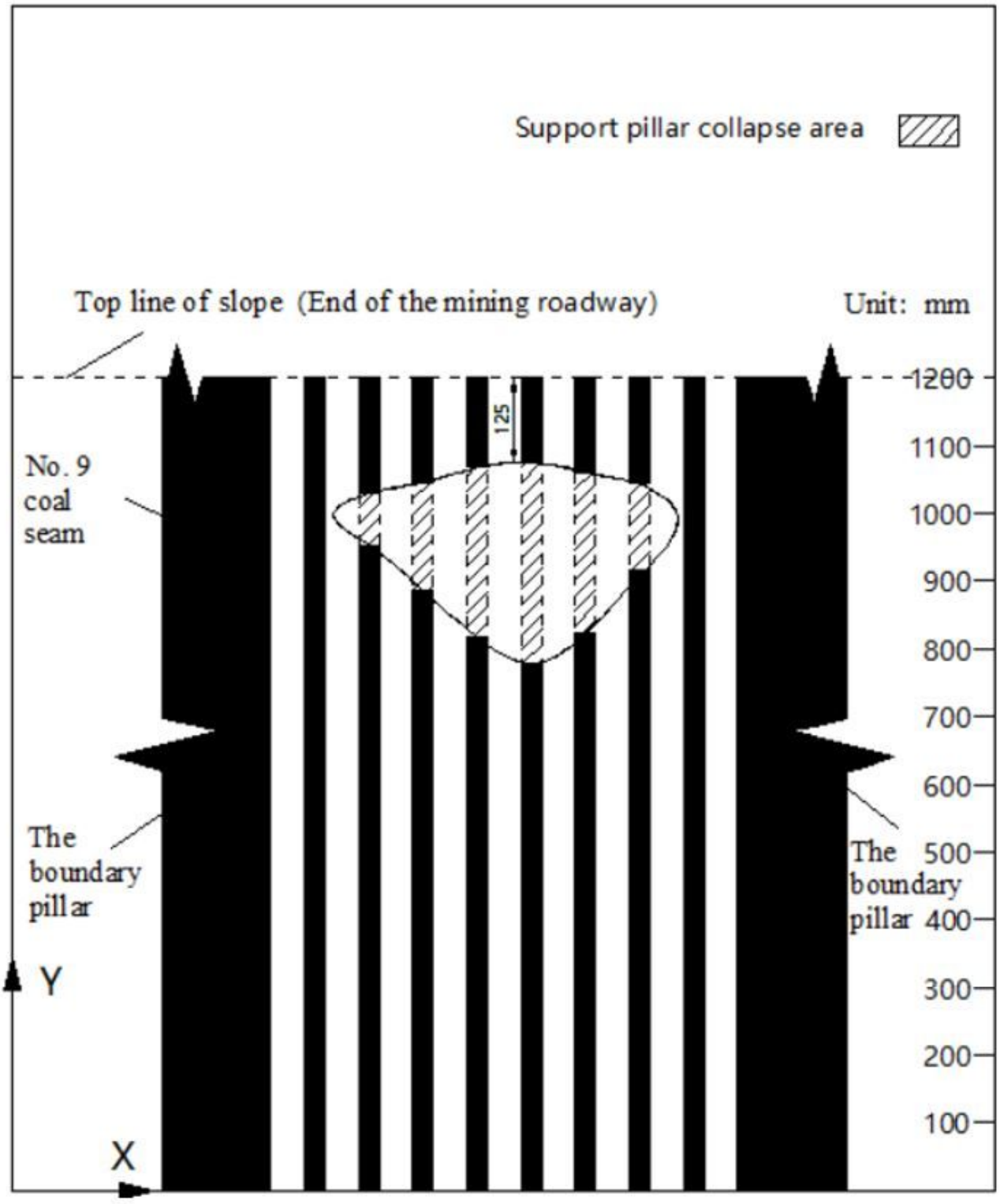

Figure 10

Diagram of the yield failure position of the supporting coal pillar

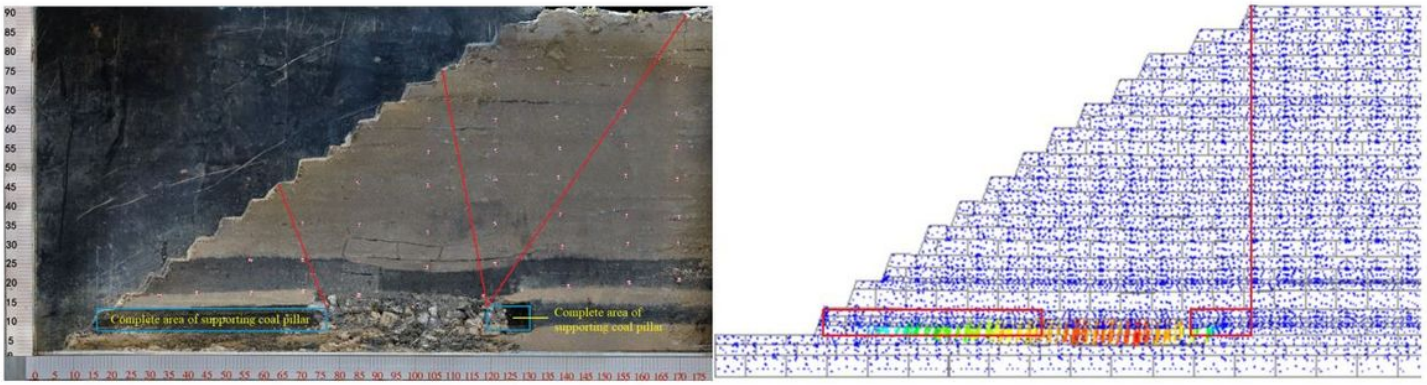

（a）Results of model experiment　　（b）Results of numerical analysis

Figure 11

Yield failure characteristics of the coal pillar about the mining slope

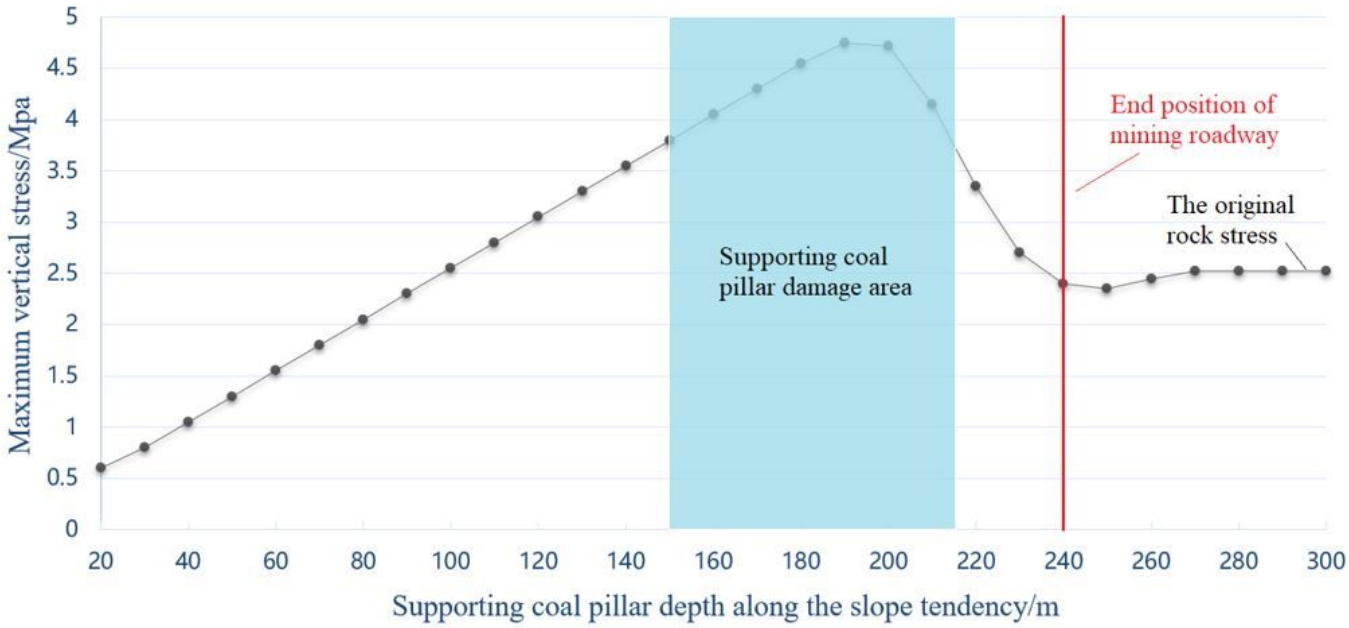

Figure 12

Vertical stress curve of the supporting coal pillar varies with mining depth

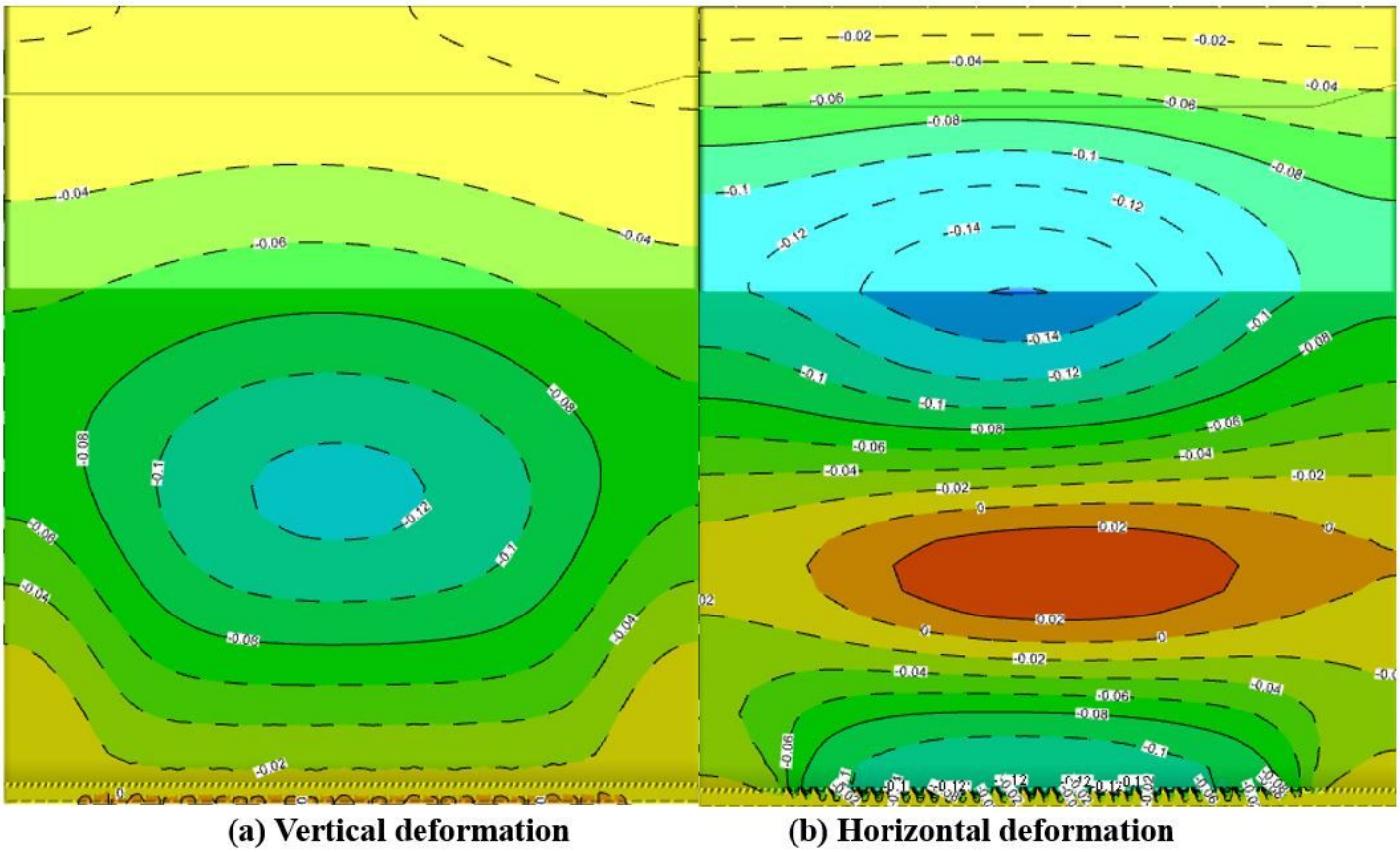

Figure 13

Cloud image of slope surface deformation (unit: cm)

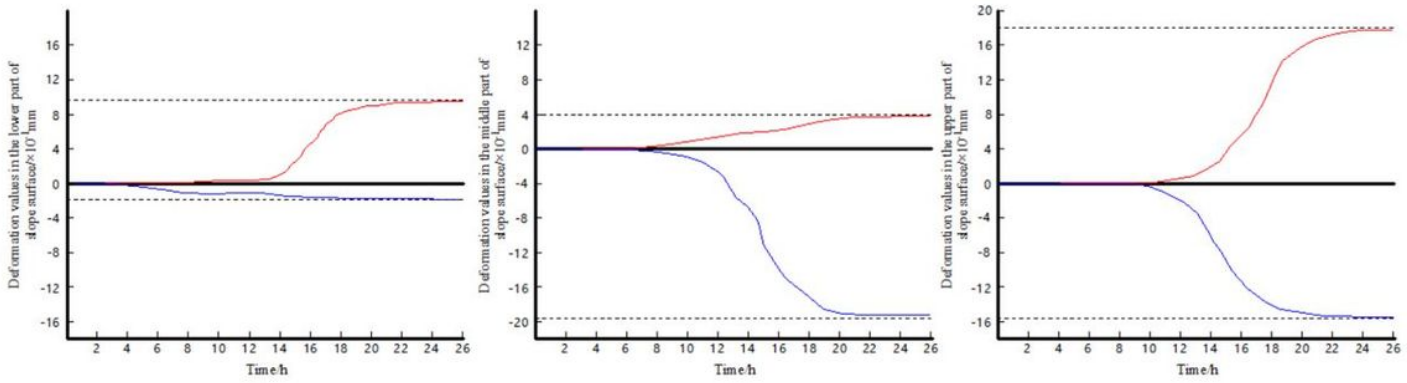

Figure 14

Deformation curve of typical displacement monitoring points on the slope surface

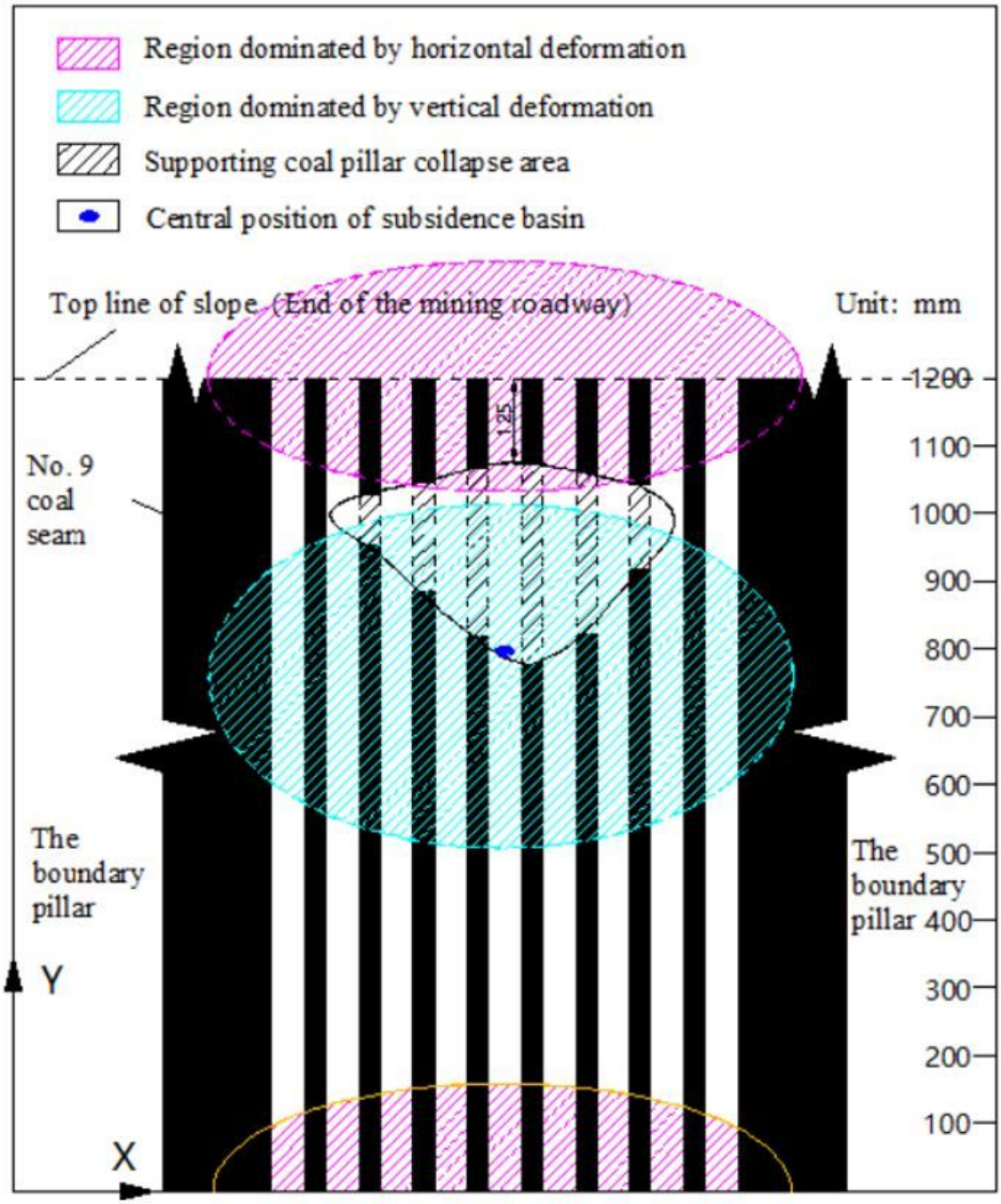

Figure 15

Diagram of the spatial correspondence between the coal pillar failure zone and the slope surface

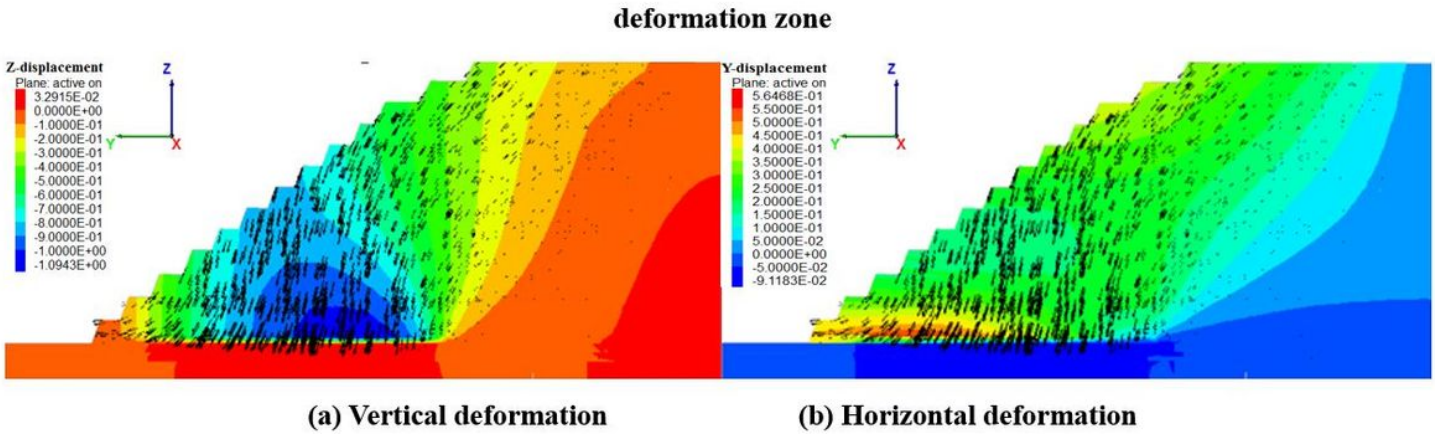

Figure 16

Deformation and failure characteristics of the rock and soil mass of the mining slope

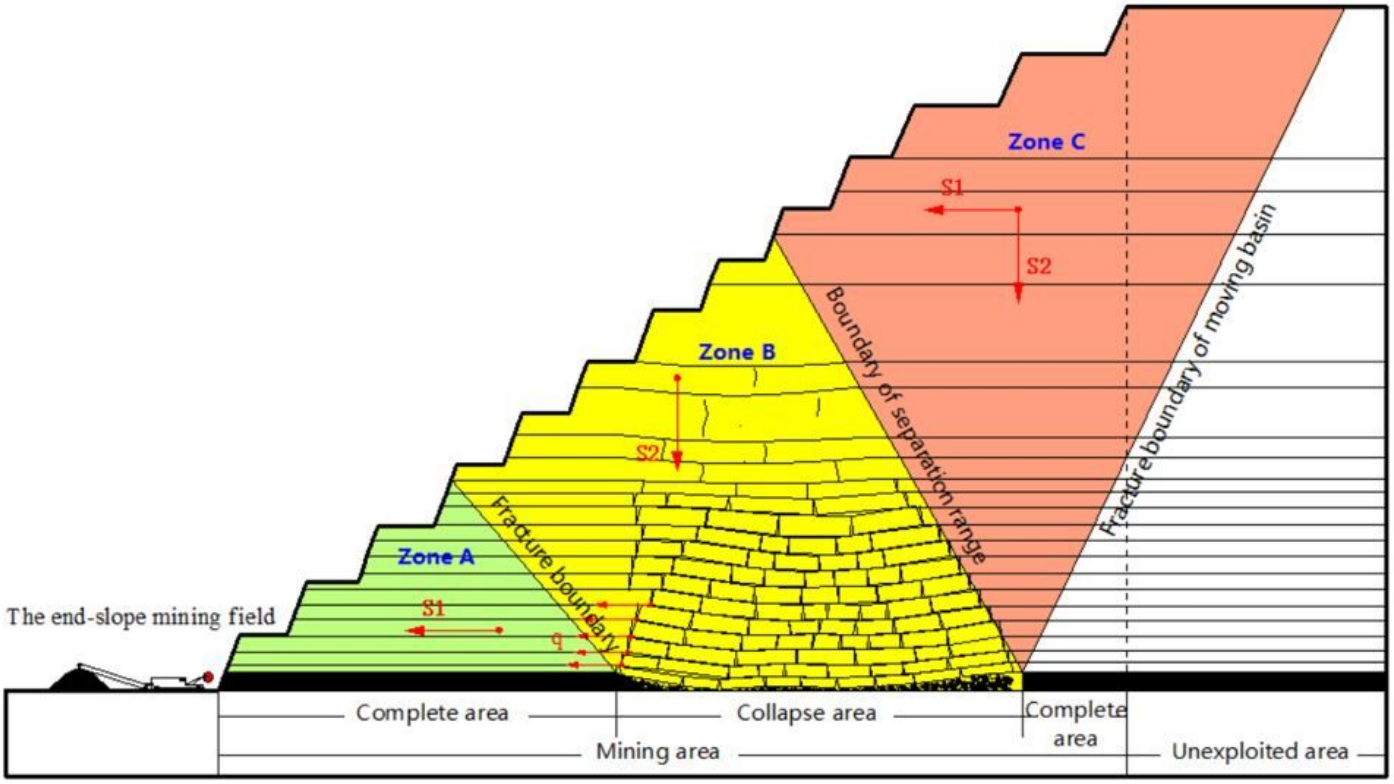

Figure 17

Deformation and failure zones of overlying rock in the end slope under the coal extraction condition